Organic Geochemistry 103 (2017) 88–96

Contents lists available at ScienceDirect

Organic Geochemistry

journal homepage: www.elsevier.com/locate/orggeochem

Branched GDGT signals in fluvial sediments of the Danube River basin: Method comparison and longitudinal evolution

Chantal V. Freymond [a,*], Francien Peterse [a,b], Lorena V. Fischer [a], Florin Filip [c,d], Liviu Giosan [e], Timothy I. Eglinton [a]

[a] Geological Institute, ETH Zürich, Sonneggstrasse 5, 8092 Zürich, Switzerland
[b] Department of Earth Sciences, Utrecht University, Heidelberglaan 2, 3584 CS Utrecht, The Netherlands
[c] Department of Geography, University of Bucharest, Bucharest, Romania
[d] Fabrica de Cercetare, Str. Olari Nr.7 Etj.2 Ap.5, Bucharest, Romania
[e] Geology & Geophysics, Woods Hole Oceanographic Institution, 266 Woods Hole Road, Woods Hole, MA 02543-1050, USA

ARTICLE INFO

Article history:
Received 14 July 2016
Received in revised form 26 October 2016
Accepted 1 November 2016
Available online 14 November 2016

Keywords:
brGDGTs
Danube River
Liquid chromatography–mass spectrometry
Method comparison
River carbon transport

ABSTRACT

Abundances and distributional changes of branched glycerol dialkyl glycerol tetraethers (brGDGTs) in fluvially influenced sediments are used in various paleoclimate studies to reconstruct variations in soil export, continental air temperature and soil pH in corresponding river basins. For accurate interpretation of these records, it is important to understand the provenance and the evolution of biomarker signals as they move through the river system. Here we investigate the brGDGT composition of modern river sediments of the Danube River, the second largest river in Europe. BrGDGT-based mean annual air temperature and soil pH parallel the actual values of air temperature and soil pH from the upper to the lower basin, showing that signals predominantly reflect local as opposed to basin-wide environmental conditions. Furthermore, data generated using the recently developed method with improved chromatography, separating the 6-methyl-isomers from the 5-methyl-isomers, was compared with that resulting from the conventional method. We show that the temperatures and pH values reconstructed using the data obtained by improved chromatography best resemble the local environmental conditions throughout the Danube River basin. Our results highlight the importance of in-depth studies within river systems to better understand the provenance of biomarker signals in fluvially derived sedimentary archives.

1. Introduction

Branched glycerol dialkyl glycerol tetraethers (brGDGTs; Fig. 1) are promising biomarkers to reconstruct paleo-environmental conditions on land (Weijers et al., 2007a; Bendle et al., 2010; Sinninghe Damsté et al., 2012; Sanchi et al., 2014, 2015). These lipids occur widely in soils and peats around the globe (Weijers et al., 2004, 2007b; Peterse et al., 2012; Ding et al., 2015). In addition to being found in soils, brGDGTs are also produced in rivers and lakes (e.g., Tierney and Russell, 2009; Weber et al., 2015). Although identifying the organisms producing brGDGTs has proven challenging, brGDGTs are likely to be membrane lipids derived from heterotrophic bacteria (Oppermann et al., 2010; Weijers et al., 2010; Huguet et al., 2013). Certain cultured *Acidobacteria* have been found to produce the tetra-methylated brGDGT Ia (Sinninghe Damsté et al., 2011), however, other bacterial strains synthesizing brGDGTs cannot be excluded and the exact source organism(s) of brGDGTs remain(s) elusive.

In general, bacteria modify their composition of cell membrane lipids for optimal function under given environmental conditions such as temperature (that influences membrane flexibility) and pH (which has an influence on the proton gradient across the cell membrane) (Weijers et al., 2007b; Sinninghe Damsté et al., 2011). Hence, variations in lipid composition can correspond to an adaptation mechanism of the microorganisms to changing environmental conditions, but can also result from changes in the microbial community composition, that are reflected in the diversity of lipids encountered (Prado et al., 1988; Suutari and Laakso, 1992; Sinninghe Damsté et al., 2011, 2014). This physiological adaptation and associated variation in biomarker lipids provides the foundation for molecular proxies to reconstruct parameters such as mean annual air temperature (MAAT) and the soil pH from the relative distributions of different brGDGTs (Fig. 1) (Weijers et al., 2007b; De Jonge et al., 2014a). The brGDGTs occur with varying amounts of (a) four to six methyl groups ('branches'), a feature

* Corresponding author.
E-mail address: Chantal.Freymond@erdw.ethz.ch (C.V. Freymond).

http://dx.doi.org/10.1016/j.orggeochem.2016.11.002
0146-6380/

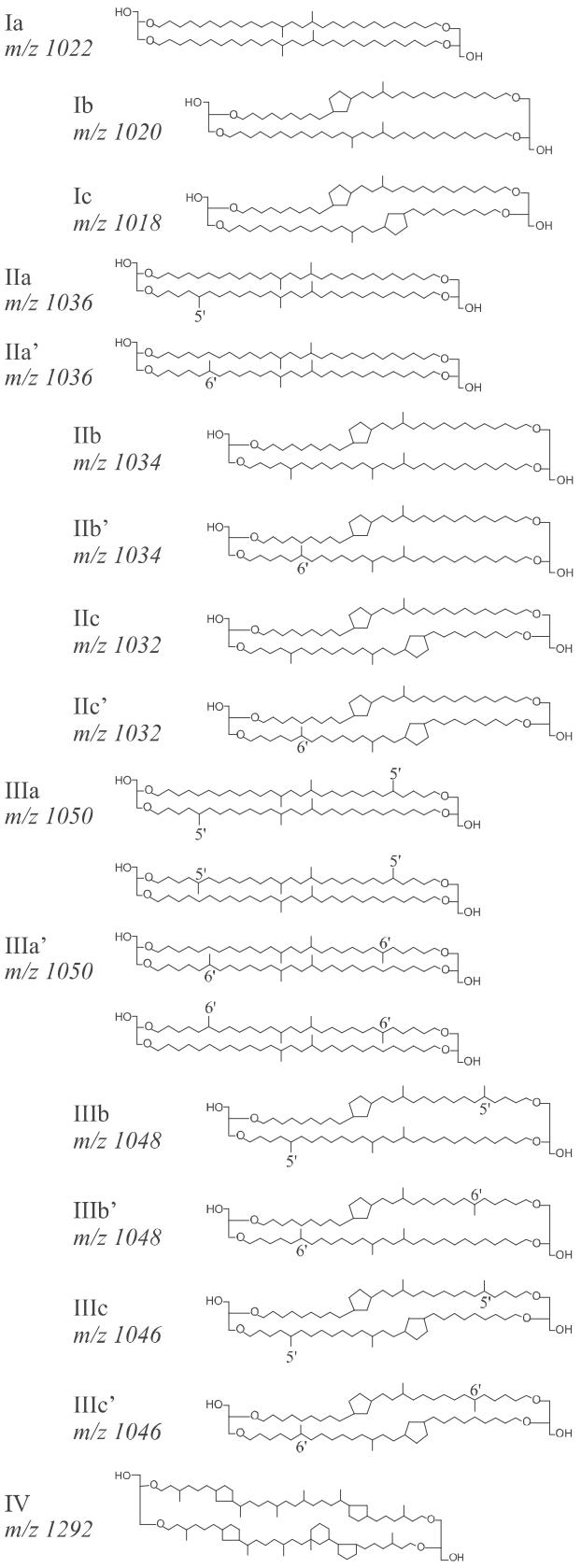

Fig. 1. Molecular structures of the branched and isoprenoid GDGTs measured in this study (De Jonge et al., 2014a).

that can be summarized by the methylation index of branched tetraethers (MBT) that correlates to mean annual air temperature and to a lesser extent to soil pH and (b) the incorporation of up to two cyclopentane moieties, expressed as the cyclization index of branched tetraethers (CBT) that co-varies with soil pH (Weijers et al., 2007b; Peterse et al., 2012). Upon soil erosion and subsequent river runoff and discharge, brGDGTs may serve as tracers of terrestrial organic matter, delivering continental climate information to shelf sediments. The relative amount of brGDGTs compared to that of crenarchaeol, an isoprenoidal GDGT produced by Thaumarchaeota that are abundant in the open ocean, is quantified by the branched to isoprenoid tetraether (BIT) index (Hopmans et al., 2004) and is used to identify soil inputs to marine sediments. The BIT index is also applicable to some freshwater systems since crenarchaeol is also produced in lacustrine environments (Schouten et al., 2013). However, the presence of crenarchaeol in soils, and the production of brGDGTs in aquatic environments may at times complicate the interpretation of the BIT index as indicator of soil input (Schouten et al., 2013).

Regardless, application of these proxies has resulted in records of continental paleotemperatures and past soil pH within river basins, on the assumption that the brGDGT load exported by the river to shelf sediments represents an integrated signal of the catchment area (Weijers et al., 2007a; Bendle et al., 2010; Sanchi et al., 2014). However, this assumption and simplification remains largely untested as the source region and transport history of exported organic carbon is not well constrained for many river systems. For example, the distribution of brGDGTs could potentially be influenced by hydrodynamic sorting or microbial reworking during fluvial transport. Furthermore, the finding that brGDGTs may also be produced in aquatic environments complicates the interpretation of proxy-based temperature, pH, and BIT records, as this in situ contribution may affect or overprint the original soil-derived brGDGT signature in a river (e.g., Tierney and Russell, 2009; Buckles et al., 2014; De Jonge et al., 2014b; Zell et al., 2014). Finally, certain brGDGT peaks have co-eluting isomers in the initial chromatographic method used to analyze brGDGTs – recognizable in the chromatogram as shoulders on the peaks – complicating peak integration and thus contributing to an error in the reconstructed environmental parameter. A recently refined chromatographic method using different columns now enables the separation of these shoulder peaks (De Jonge et al., 2014a; Hopmans et al., 2016), which were found to be brGDGT isomers with a methyl group at the α6 and/or ω6 instead of the α5 and/or ω5 position (Fig. 1) (De Jonge et al., 2013), and shown to correlate with soil pH (De Jonge et al., 2014a; Xiao et al., 2015) and soil moisture content (Dang et al., 2016). Subsequent recalibration of the MAT and pH transfer functions for the global soil calibration data set resulted in improved correlations, reducing the residual mean error on brGDGT-based temperatures and soil pH from 5 °C to 4.6 °C and from 0.8 to 0.5, respectively (Peterse et al., 2012; De Jonge et al., 2014a). Using the new chromatography method, De Jonge et al. (2014b) revealed that 6-methyl brGDGTs dominated the brGDGTs in suspended particulate matter (SPM) carried by the Yenisei River. Similarly, Weber et al. (2015) identified a novel isomer of brGDGT-IIIa with methylations on the 5 and 6′ positions in a suite of Swiss lakes. The absence of this compound in surrounding soils and its distinct $\delta^{13}C$ signature confirm the production of brGDGTs in aquatic environments. Hence, in addition to the improved accuracy, the novel chromatography method may also provide information on possible contributions of in situ produced brGDGTs when used in studies tracing fluvial transport of soil organic matter.

In this study, a detailed basin-wide investigation of the brGDGT composition of modern fluvial sediments along the Danube River is undertaken. In order to understand the composition, provenance, and transport history of the brGDGT signal that is finally exported to the Black Sea, the changes in brGDGT abundances and distributions were examined from headwater tributaries to the Danube

delta. Furthermore, data obtained using the "classic" GDGT measurement method and soil calibration (Schouten et al., 2007; Peterse et al., 2012) are compared with those using the method with improved chromatography (De Jonge et al., 2014a; Hopmans et al., 2016) to assess the potential of the latter method to identify the contribution of aquatic production to the total brGDGT pool present in river sediment deposits.

2. Site description

The Danube River (Fig. 2A) is the largest river of the European Union (catchment area: 801,463 km^2; length: 2850 km). With its source in the Black Forest, southern Germany, and its terminus in the Black Sea, the Danube has a general west to east orientation, and can be divided into three geographic regions: the upper basin from the source to the Gate of Devin (transverse valley between the Eastern Alps and the Little Carpathians) east of Vienna (border Austria/Slovakia), the middle basin from the Gate of Devin to the Iron Gates reservoir where the Danube cuts the Carpathian Mountains, and the lower basin downstream of the Iron Gates (Fig. 2A). The upper basin is influenced by an Atlantic climate with high precipitation, whereas dry and cold winters and higher temperatures in summer are typical for the continental climate that characterizes the eastern part of the basin (ICPDR, 2005). The southwest, i.e., the Drava and Sava catchments, is partly influenced by a Mediterranean climate with less precipitation in summer (ICPDR, 2005; McCarney-Castle et al., 2012). In short, mean annual air temperature in the upper, middle, lower basin, and the delta is 6.7 °C, 8.8 °C, 9.2 °C, 10.7 °C, mean annual precipitation is 1012 mm, 792 mm, 605 mm, and 432 mm, mean suspended solids are 27.5 mg/L, 29.0 mg/L, 43.7 mg/L, and 36.1 mg/L (Tockner et al., 2009), and the average soil pH is 6.4, 6.3, 6.7, and 5.1 (Fig. 2B), respectively. The Danube basin has experienced a long history of human influence since the Neolithic as agriculture spread into Europe along the river and its tributaries. Deforestation started early in the upper basin, and reached around 30% during the peak of the Roman Empire. In the lower basin, deforestation rapidly increased after 1000 years AD, resulting in enhanced soil erosion and suspended sediment load (Giosan et al., 2012). With subsequent industrialization, inorganic nitrogen and phosphorus load increased, leading to eutrophication of the river, floodplains and the Black Sea (Kideys, 2002; Giosan et al., 2012). Training and damming of the Danube and its tributaries started in the 1870s. Following the construction of the largest hydropower dams, Iron Gate I (1972) and Iron Gate II (1986) downstream of the Carpathian Mountains, the sediment load of the lower Danube basin was reduced by approximately 50% (McCarney-Castle et al., 2012).

3. Methods

3.1. Sampling

Along a stretch of more than 2200 km, river sediments were collected from the flanks of the river at 15 sites along the Danube mainstream and of the 12 largest tributaries between Passau (Germany) and the Black Sea (Fig. 2; Supplementary Table S1) during May and June 2013. "River sediment" is defined here as recently accumulated sediment from the riverbank or in very calm and shallow water deposited during decreasing water level following the last high water event. The fine fraction (< 63 μm) of this river sediment is considered to represent an integrated signal of the SPM of the river during the deposition period.

Notably, during the sampling campaign, a heavy rain event impacted central Europe with precipitation of up to > 100 mm within three days for large parts of the upper basin. This corresponds to more than 100% of the average May precipitation (Grams et al., 2014) and caused a 100-year flood event in the upper and middle basin (ICPDR, 2014). High water levels and flood deposits of mostly coarse sandy sediments complicated the sampling and rendered it impossible to find freshly deposited fine-grained river sediments at several planned locations in the upper and middle basin.

Nevertheless, river sediments were collected from the following tributaries: Inn, Enns, Morava, Vah, Drava, Tisa, Sava, Velika Morava, Jiu, Olt, Siret and Prut (n = 12; Fig. 2). Corresponding sediments from the Danube mainstream (n = 15) were collected immediately before and within ~5 km after the confluence of these tributaries and the mainstream, from sites with quiescent hydrodynamic conditions where fine-grained sediment (~ < 1 mm grain size) accumulated. At every location where fine sediment was available, approximately 2 kg of surface sediment was transferred to ziplock bags. The sediment samples were kept frozen until further treatment in the laboratory at ETH Zürich.

3.2. Sample processing and extraction

Bulk river sediments were wet sieved with milliQ water over 200 μm and 63 μm sieves on a shaking table. The resulting < 63 μm fraction was freeze-dried and kept frozen until subsequent sample work-up.

30–50 g of dry < 63 μm bank sediments were microwave-extracted with dichloromethane/methanol (DCM/MeOH, 9:1, v:v, 25 min at 100 °C). A 5% aliquot of the resulting total lipid extract (TLE) was saponified with KOH in MeOH (0.5 M, 2 h at 70 °C) to allow for analysis of other biomarkers (e.g., fatty acids) in the same extract. After the addition of 5 mL MilliQ water with NaCl the neutral phase was back-extracted with hexane (Hex) and further separated by eluting over a 1% deactivated SiO_2 column into: (1) an apolar fraction with Hex:DCM (9:1, v:v) and (2) a polar fraction (containing the GDGTs) with DCM:MeOH (1:1, v:v). The GDGT fraction was dissolved in Hex/isopropanol (Hex/IPA, 99:1, v:v) and passed over 0.45 μm PTFE filters. For quantification, 0.115 μg of an internal C_{46} GDGT standard (Huguet et al., 2006) was added.

3.3. GDGT analysis

3.3.1. The classic HPLC–APCI–MS method

The GDGT fractions were dissolved in Hex:IPA (99:1, v:v) and analyzed at ETH Zürich using a Agilent 1260 High Performance Liquid Chromatograph with Atmospheric Pressure Chemical Ionization coupled to a quadrupole Mass Spectrometer (HPLC–APCI–MS) according to Schouten et al. (2007). GDGTs were separated over a Grace Prevail cyano column (150 mm × 2.1 mm, 3 μm), preceded with a guard column with the same packing. Injection volume was 10 μL and the flow rate was set to 0.2 mL/min. The samples were eluted for 5 min with 90% Hex, 10% Hex:IPA (9:1, v:v), followed by a linear relative increase in Hex:IPA (9:1, v:v) to 82% Hex, 18% Hex:IPA over 34 min. Between samples, a 10 min back-flush phase with Hex:IPA (9:1, v:v), and a 10 min equilibrium phase with Hex:IPA (99:1, v:v), was set up.

3.3.2. The UHPLC–APCI–MS method with improved isomer separation

The GDGT fractions were dissolved in Hex:IPA (99:1, v:v) and separated on a Ultra High Performance Liquid Chromatograph (Agilent 1290) coupled to an Agilent 6310 quadrupole Mass Spectrometer (UHPLC–APCI–MS) at Utrecht University. Two silica Waters Acquity UPLC HEB Hilic (1.7 μm, 2.1 × 150 mm) columns, preceded by a guard column of the same material, were used for separation of the GDGTs. The injection volume was set to 10 μL and the flow rate to 0.2 mL/min. The samples were eluted with 82% Hex, 18% Hex:IPA (9:1, v:v) for 25 min, followed by a linear

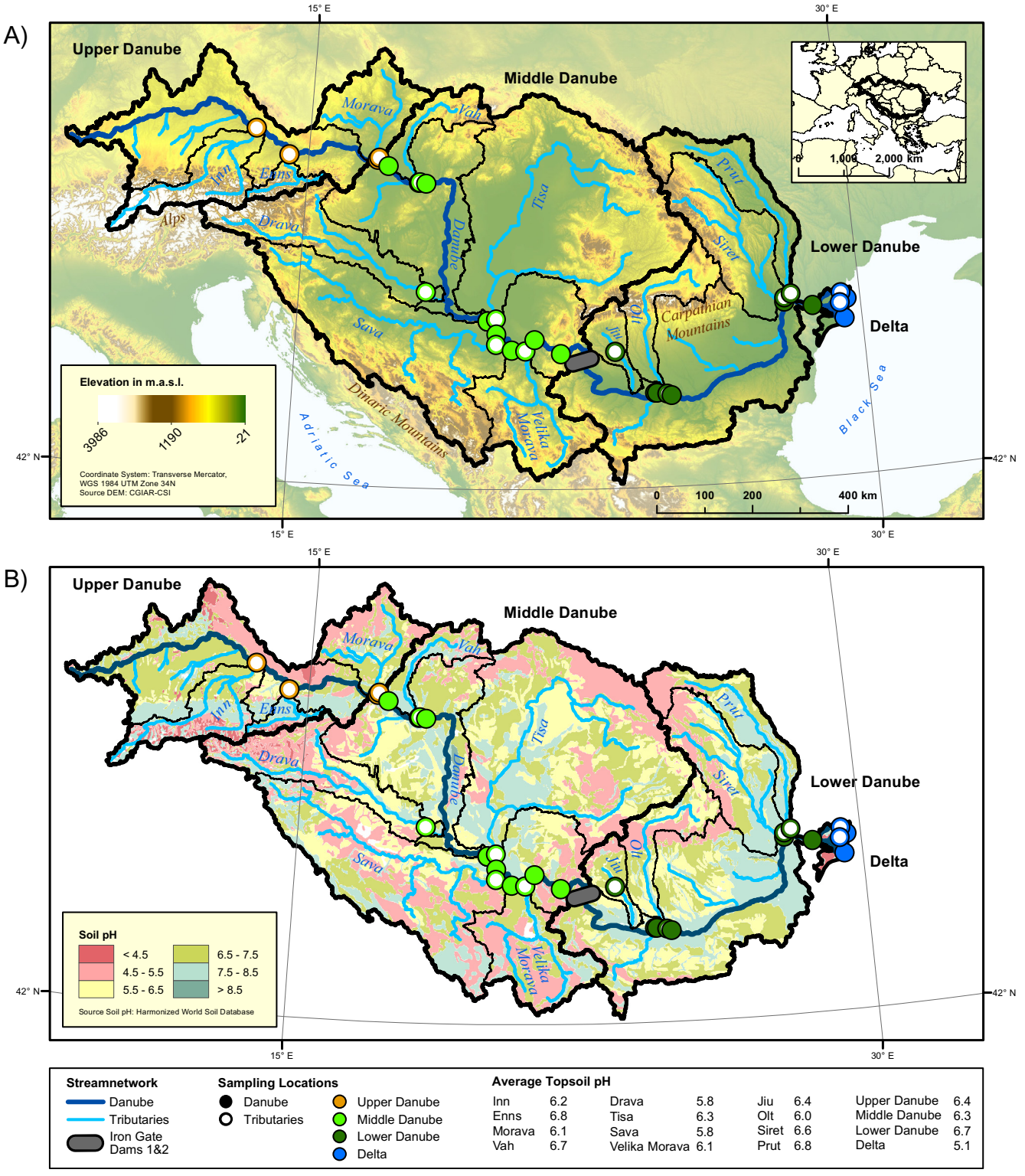

Fig. 2. (A) The Danube River catchment. Sampling locations are shown as closed symbols for the Danube main branch and open symbols for tributaries, with the upper, middle, lower basin and delta indicated in orange, light green, dark green and blue, respectively. The border of the drainage basin is shown with a thick black line, as are the borders of the sub-basins. Tributary catchments borders are shown in thin black lines. The locations of two Iron Gate dams are indicated as a single gray bar. (B) Top soil pH map of Eastern Europe covering the Danube catchment. Data from the Harmonized World Soil Database (HWSD, 2012). (For interpretation of the references to color in this figure legend, the reader is referred to the web version of this article.)

gradient to 70% Hex, 30% Hex:IPA (9:1, v:v), for 25 min, and then to 100% Hex:IPA (9:1 v:v) in 30 min. Each run was followed by a 20 min equilibration phase (Hopmans et al., 2016).

Both HPLC systems were operated in selected ion mode (SIM). The following $[M+H]^+$ ions were detected: *m/z* 1292, 1050, 1048, 1046, 1036, 1034, 1032, 1022, 1020, 1018 and 744 for the internal

standard. Molecular structures corresponding to the *m/z* values are depicted in Fig. 1.

3.4. Proxy calculation

GDGT-based proxies were calculated using the following equations for data generated using the classic method. Apparent shoulders were generally cut off during the integration step.

$$BIT = (Ia + IIa + IIIa)/(Ia + IIa + IIIa + Cren) \quad (1)$$

(Hopmans et al., 2004)

$$MBT' = (Ia + Ib + Ic)/(Ia + Ib + Ic + IIa + IIb + IIc + IIIa) \quad (2)$$

(Peterse et al., 2012)

$$CBT = -\log[(Ib + IIb)/(Ia + IIa)] \quad (3)$$

(Weijers et al., 2007b)

$$pH = 7.90 - 1.97 \times CBT \quad (r^2 = 0.70,\ RMSE = 0.8) \quad (4)$$

(Peterse et al., 2012)

$$MAT = 0.81 - 5.67 \times CBT + 31.0 \times MBT' \quad (r^2 = 0.59,\ RMSE = 5.0\ ^\circ C) \quad (5)$$

(Peterse et al., 2012)

For the data generated using the method with improved chromatography, the following transfer functions were used to calculate the proxy values:

$$BIT = (IIIa + IIIa' + IIa + IIa' + Ia)/(IIIa + IIIa' + IIa + IIa' + Ia + Cren) \quad (6)$$

(Hopmans et al., 2004; De Jonge et al., 2015)

$$\text{Fractional abundance of each compound: rel-x} = x/(Ia + Ib + Ic + IIa + IIa' + IIb + IIb' + IIc + IIc' + IIIa + IIIa' + IIIb + IIIb' + IIIc + IIIc'), \quad (7)$$

where x stands for one of the brGDGTs.

$$CBT' = \log_{10}[(\text{rel-Ic} + \text{rel-IIa}' + \text{rel-IIb}' + \text{rel-IIc}' + \text{rel-IIIa}' + \text{rel-IIIb}' + \text{rel-IIIc}')/(\text{rel-Ia} + \text{rel-IIa} + \text{rel-IIIa})] \quad (8)$$

(De Jonge et al., 2014a)

$$MAT_{mr} = 7.17 + (17.1 \times \text{rel-Ia}) + (25.9 \times \text{rel-Ib}) + (34.4 \times \text{rel-Ic}) - (28.6 \times \text{rel-IIa}) \quad (r^2 = 0.68,\ RMSE = 4.6\ ^\circ C) \quad (9)$$

(De Jonge et al., 2014a)

$$pH = 7.15 + 1.59 \times CBT' \quad (r^2 = 0.85,\ RMSE = 0.52) \quad (10)$$

(De Jonge et al., 2014a)

$$IR = (IIa' + IIb' + IIc' + IIIa' + IIIb' + IIIc')/(IIa + IIb + IIc + IIIa + IIIb + IIIc + IIa' + IIb' + IIc' + IIIa' + IIIb' + IIIc') \quad (11)$$

(De Jonge et al., 2015).

3.5. Average soil pH calculation

The soil pH map was downloaded from the Harmonized World Soil Database (HWSD, 2012) and imported to ArcGIS (version 10.2.2). The pH value for each layer (originally representing a range of 1 pH unit) was set to the mean value (e.g., the layer pH 4.5–5.5 was set to pH 5). The average soil pH value (calculated with the function 'Zonal Statistics Table') for each Danube sampling location was calculated from the catchment area that lays in between the considered location and the one more upstream. First, the drainage area for the considered location was calculated, which includes the entire catchment upstream of this point. Then, the drainage area for the sampling location upstream of the considered location was calculated in the same way. The intermediate area was finally obtained by subtracting the catchment area from each other (downstream minus upstream location). Average intermediate area pH was chosen for comparison with brGDGT-derived pH values because it represents the local soil contributions. Average soil pH values for tributary sampling locations represent the average of the entire tributary catchment area.

4. Results

4.1. Classic method

Chromatograms from the classic method show clear shoulders on the brGDGT-IIIa, IIIb and IIIc peaks that correspond to the 5-methyl (left shoulder) and the 6-methyl (right shoulder) isomers. These 6-methyl shoulders are often comparable in size as the presumed 5-methyl brGDGT-IIIa, IIIb and IIIc peaks, respectively (Supplementary Fig. S1). No shoulders, and thus no isomers were visible for the peaks corresponding to brGDGT IIa–c.

The brGDGT-derived temperatures based on brGDGTs measured with the classic method and transfer functions of Peterse et al. (2012) are in the same range for the upper and middle basin (Fig. 3A, Supplementary Table S1), and increase after the Iron Gates reservoir. Reconstructed MAT values for the Danube plus tributaries range from 4.9 °C to 10.9 °C (average MAT = 7.3 °C, $n = 32$) and from 4.9 °C to 8.5 °C (average MAT = 7.1 °C, $n = 18$) only for sampling locations in the Danube mainstream (Fig. 3A, Supplementary Table S1). Calculated soil pH values after Peterse et al. (2012) based on this method tend to increase from 6.7 to 7.5 (average pH = 7.2, $n = 32$) for the Danube plus tributaries and from 7.0 to 7.4 (average pH = 7.2, $n = 18$) only for the Danube locations (Fig. 3A, Supplementary Table S1). Corresponding BIT index values including the tributaries range from 0.81 to 0.95 with an average of 0.90 ($n = 32$), and from 0.83 to 0.94 with an average of 0.90 ($n = 18$) excluding the tributaries (Fig. 3A, Supplementary Table S1).

4.2. Method with improved chromatography

Using the improved chromatography method with two silica columns, all six 6-methyl isomers (IIIa′–IIIc′ and IIa′–IIc′) were detected and appeared clearly separated from the 5-methyl isomers in every chromatogram, in similar abundance as the 5-methyl brGDGTs (Supplementary Fig. S1).

Reconstructed temperatures (Fig. 3B, Supplementary Table S1) range from 5.7 °C to 11.1 °C (average MAT_{mr} = 7.9 °C, $n = 32$) for the Danube plus tributaries, and steadily increase from 6.9 °C to 9.1 °C (average MAT_{mr} = 7.8 °C, $n = 18$) for the Danube mainstream excluding tributary sampling locations (Fig. 3B, Supplementary Table S1). Average MAT_{mr} values for the sub-basins are 6.7 °C, 7.4 °C, 8.8 °C and 8.7 °C for the upper, middle, lower basin and the delta, respectively. Calculated soil pH values after De Jonge et al. (2014a) are between 6.9 and 7.5 (average pH = 7.2, $n = 32$) and between 7.2 and 7.5 (average pH = 7.3, $n = 18$) excluding tributaries (Fig. 3B, Supplementary Table S1). The BIT values of the Danube mainstream and tributaries ($n = 32$) show consistently high values, ranging from 0.76 to 0.95 with an average of 0.89 (Fig. 3B, Supplementary Table S1). The lowest BIT values (0.76 and 0.78) are from an old, unchannelized distributary in the Danube Delta and a tributary in the lower basin (Olt River), respectively. Excluding tributaries, BIT values for the Danube mainstream

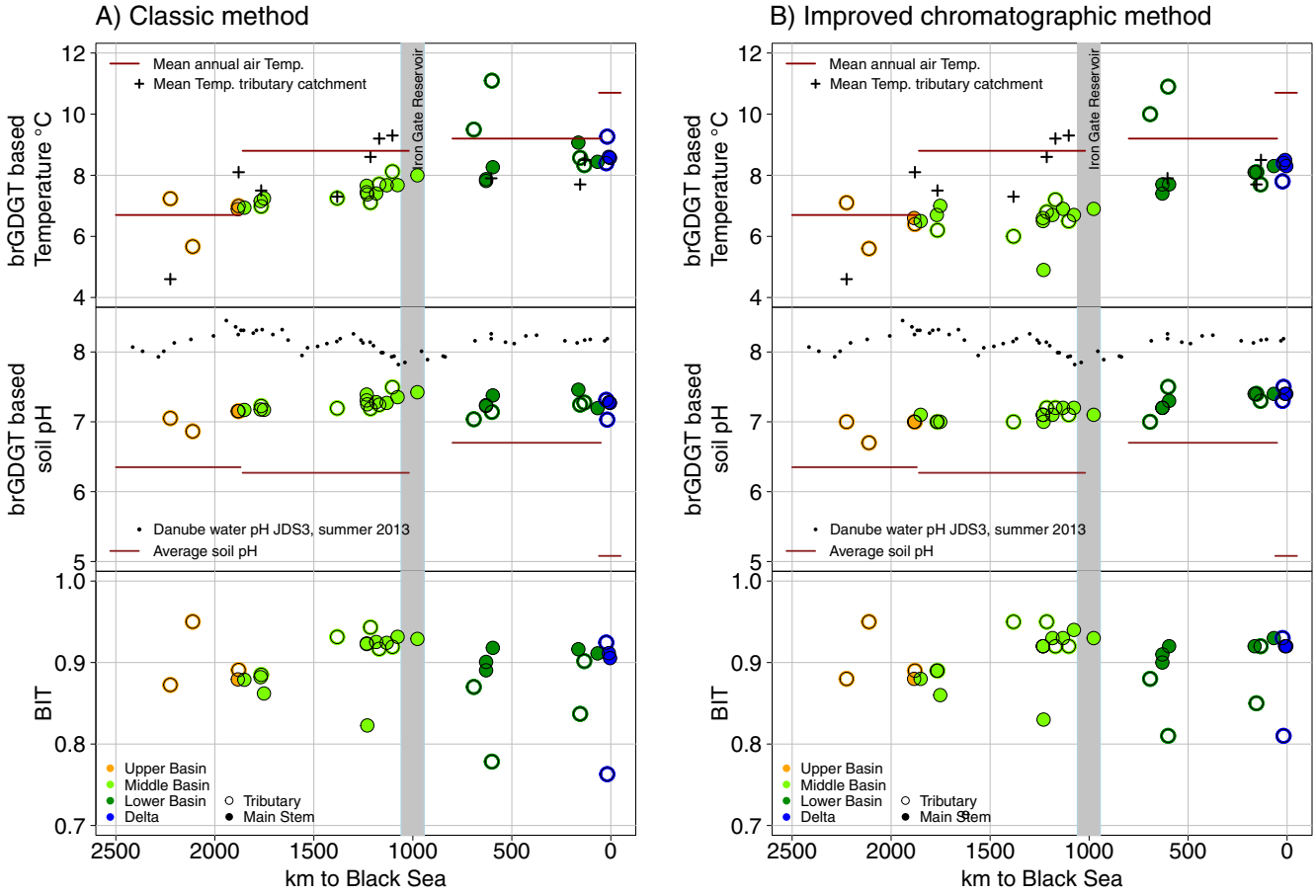

Fig. 3. Br-GDGT based mean annual air temperature, soil pH and BIT index determined by (A) the classic method and (B) the method with improved chromatography. Open circles are sampling locations at tributaries; closed circles are sampling locations at the Danube mainstream. Symbol colors correspond to those in Fig. 2. The vertical gray bar shows the location of the Iron Gate reservoir. Actual mean annual air temperatures of sub-basins and tributary catchments are from Tockner et al. (2009); Danube water pH is from the Joint Danube Survey 3, Summer 2013 (JDS3, 2013); for average soil pH see Fig. 2B. (For interpretation of the references to color in this figure legend, the reader is referred to the web version of this article.)

are between 0.82 and 0.93 with an average value of 0.90 ($n = 18$) (Fig. 3B, Supplementary Table S1).

4.3. Method comparison

For a comparison of the two methods, proxy values of the classic method are plotted against those from the improved chromatography method (Fig. 4A–E). MAT, BIT, total brGDGT concentration, and crenarchaeol concentration show linear correlations with r^2 values of 0.79, 0.95, 0.95 and 0.95, respectively. The improved method generally returns slightly higher MAT values (average +0.6 °C), whereas brGDGT and crenarchaeol concentrations are on average 34% and 26% lower compared to the classic method. Notably, there is no correlation between brGDGT-derived pH values reconstructed using the two methods ($r^2 = 0.09$), although this is likely caused by the limited pH range (0.8; 0.6 pH unit for the classic and the improved chromatography method, respectively) covered by the samples.

5. Discussion

5.1. Method comparison

The use of the new method revealed the presence of 6-methyl isomers for brGDGT IIa–IIc that were not visible in the chromatograms obtained with the classic method (Supplementary Fig. S1). As a consequence, for the latter, these isomers are automatically included during derivation of proxy values (Eqs. (1)–(5)).

The brGDGT and crenarchaeol concentrations measured in two different labs (ETH Zürich and Utrecht University) are very similar ($r^2 = 0.95$), albeit with generally lower concentrations measured with the improved chromatography method than with the classic method (Fig. 4D and E). This may reflect different response factors of the two mass spectrometers used (Schouten et al., 2009) or a greater loss (irreversible binding) to the HPLC column phases with the improved method compared to the classic method because of the higher column surface area. However, with the use of an internal standard, the latter should not be a factor, and indeed consistent BIT values suggest that the data acquired using two different HPLC–MS systems are comparable. Differences in calculated proxy values depending on brGDGT ratios are therefore not considered to result from use of two different HPLC–MS systems.

The brGDGT-derived MAT values from the two methods are linearly correlated (Fig. 4A), albeit with greater variability ($r^2 = 0.79$) than the BIT index (Fig. 4C) or GDGT concentrations (Fig. 4D and E). This variability may be a result of the improved separation of 6-methyl brGDGT isomers. Temperatures from the improved method are slightly higher than temperatures derived from the classic method (on average 0.3 °C, 0.9 °C, 0.3 °C and 0.5 °C for the upper, middle, lower basin, and the delta, respectively; Supplementary Table S1) and closer to the actual mean annual air temperature (c.f. Tockner et al., 2009; Fig. 3). The largest

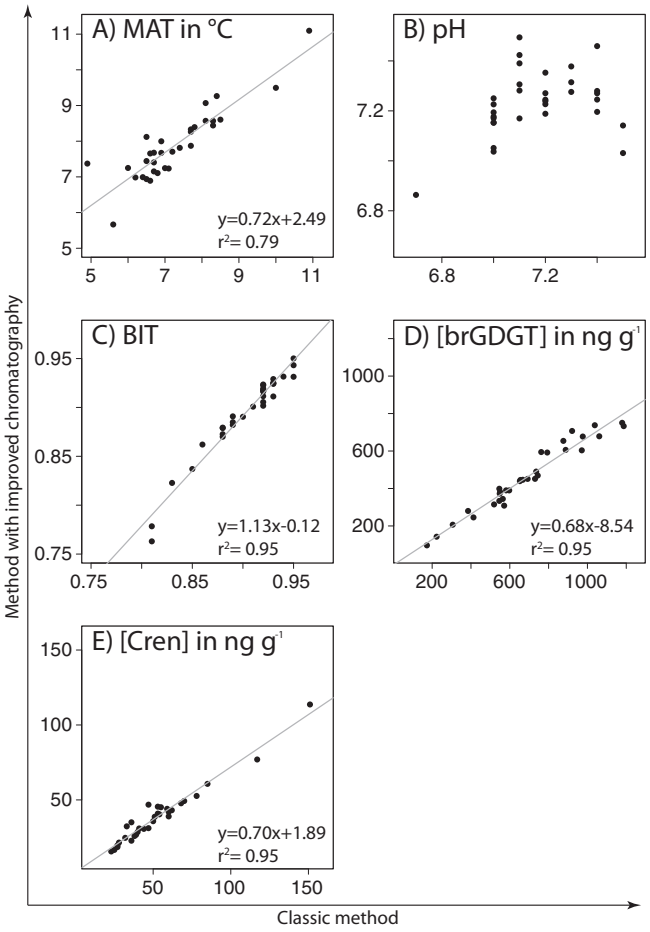

Fig. 4. Method comparison: (A) brGDGT-based mean annual air temperature, (B) brGDGT-based soil pH, (C) BIT index, (D) summed brGDGT concentration, (E) crenarchaeol concentration of the classic method against the improved chromatographic method.

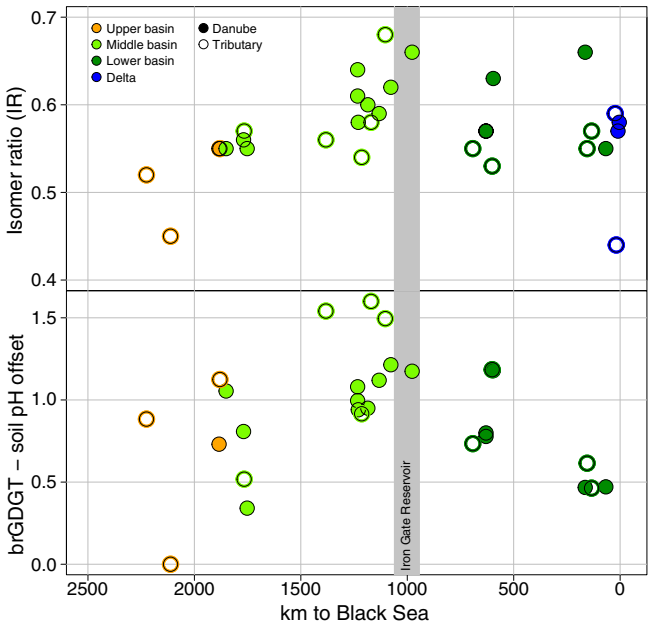

Fig. 5. Upper panel: isomer ratio (IR) showing the fractional abundance ratio of 6 methyl brGDGTs compared to total penta- and hexamethylated brGDGTs. Symbol shape and color correspond to those in Fig. 2. Lower panel: Offset between brGDGT based pH and actual soil pH along the Danube. Symbol shape and color correspond to those in Fig. 2. (For interpretation of the references to color in this figure legend, the reader is referred to the web version of this article.)

difference appears in the middle basin, where MAT_{mr} is on average 0.9 °C higher than MAT. Indeed, this offset, although it is still a very small offset, coincides with a relative increase in 6-methyl compounds compared to the 5-methyl compounds and therefore higher isomer ratio (Fig. 5), confirming its presumed influence on MAT reconstruction using the classic method. The influence of 6-methyl brGDGTs does not manifest itself comparing the pH values obtained by the two methods, as the values plot in the same limited range (pH range 6.7–7.5; Fig. 4B), implying similar reconstructed pH values for the two methods. Nevertheless, soil pH in the Danube catchment is in the range 5.8–6.8 (Fig. 2B), indicating that both methods record the same offset with actual soil pH.

Overall, we conclude that the separation of 5-methyl and 6-methyl brGDGTs improves the reliability of the generated proxy data for this river system. The subsequent discussion of brGDGT distributions in Danube River sediments therefore focuses exclusively on the results from the new method with improved chromatography.

5.2. Evolution of brGDGT distributions along the Danube

The brGDGT composition of Danube River sediments was determined with the goal of exploiting it as a tracer to study the transport of soil-derived material along the course of a major modern river system, with the working assumption that soil is the main source of brGDGTs to the river sediment. Although the range of reconstructed temperatures and pH values is relatively minor (5.4 °C; 0.6 pH; Supplementary Table S1), MAT_{mr} follows the increase in actual air temperature from headwater tributaries in the Alps to the lowlands and the Black Sea (Tockner et al., 2009) (Fig. 3B). The brGDGT-derived temperatures for the Danube main branch are – except of the upper basin – slightly lower than the actual temperatures (average offset: 0 °C; −1.4 °C; −0.4 °C and −2 °C for the upper, middle, lower basin and delta). Although this offset is well within the calibration error (4.6 °C; De Jonge et al., 2014a), there are two processes that may have contributed to the slight underestimation of MAT_{mr}: First, the sediment collected at a specific location along the river includes sediment from the upstream (cooler) part of the catchment, and will thus result in a lower reconstructed temperature than actual MAAT. This interpretation is supported by the fact that the average MAT_{mr} for the upper basin (6.7 °C) exactly matches with the actual mean annual air temperature (6.7 °C) of that sub-basin. Further, the contribution of an upstream signal is apparent in the middle basin (Fig. 3B). This river section may have received an exceptional contribution of material from the upper basin due to the 100-year flood event that occurred days before sample collection.

A second explanation is a contribution of in situ produced brGDGTs that has altered the soil-derived signal. Upstream of the Iron Gate dams, the offset in reconstructed vs actual MAAT is pronounced (Fig. 3B). The dams lower the flow velocity and decrease the turbidity of the river, promoting conditions for in situ production. A similar scenario has been described to explain brGDGT signals in front of the Three Gorges Dam in the Yangtze River (Yang et al., 2013). It is found that brGDGTs produced in lakes can cause an underestimation of MBT-CBT derived temperatures by up to 10–15 °C compared to that reflected by brGDGTs in catchment soils (Tierney and Russell, 2009; Tierney et al., 2012; Li et al., 2016). Similarly, the brGDGT composition of SPM from the Amazon River resulted in reconstructed MAT that was ~2 °C lower than that reconstructed for soils in the river catchment, and ~5 °C less than actual measurements of MAAT (Zell et al., 2013). Part of such a

'cold bias' may potentially be explained by an increased contribution of the 6-methyl isomers in freshwater systems, as brGDGTs produced in a river would record the generally higher pH of river water compared to that of soils. Using the original chromatography method, the resulting larger contribution of 6-methyl brGDGTs then causes an overestimation of their similarly eluting 5-methyl counterpart, thus introducing the described bias. This suggests that we may use the relative abundance of 6-me brGDGTs as indicator of potential in situ production. The new chromatography method and associated transfer functions (De Jonge et al., 2014a) has the advantage that functions for pH and MAT are independent. Thus, pH-induced in situ production should have a smaller effect on MAT reconstruction than when using the classic method.

Changes in the relative contribution of 6-methyl brGDGTs along the Danube are reflected by the isomer ratio (IR). This ratio is indeed slightly higher upstream of the Iron Gates (Fig. 5), which is consistent with the suggestion of enhanced in situ production in this region. However, input of local soil material with a high pH value would have a similar effect. In an attempt to disentangle the contributions of aquatic and soil-derived brGDGTs, we compared brGDGT-based pH and actual soil pH. Depicting the offset between these two pH values reveals a similar picture to that of the IR ratio, with an increased offset in front of the Iron Gate dams (Fig. 5). The average soil pH in the catchment remains relatively constant (pH = 6.3–6.4 in upper and middle basin), and only slightly increases in the lower basin (average pH = 6.7; Fig. 2B). BrGDGT-based pH values upstream of the Iron Gate dams deviate from this trend by up to 1.2 pH units, implying that the offset is indeed related to a contribution of aquatic brGDGTs. Nevertheless, the good fit of actual mean air temperature and MAT_{mr} (Fig. 3) suggests that the influence of in-river production on temperature estimates is relatively minor even in this section of the river.

The largest offset in temperature is found in the delta, where there is a 2.0 °C difference between reconstructed MAT_{mr} and actual MAAT. The delta has a west-east extension of about 80 km and contains an extensive network of small channels and connected shallow lakes, which may promote in situ production. However, we speculate that the flow path of the Danube through the delta (~90 km) is insufficient for local inputs to severely overprint the Danube signal that is entering the delta region and exported to the Black Sea. Furthermore, the consistently high BIT index values along the river indicate that the relative proportion of brGDGTs and crenarchaeol remains constant, and therefore points to a single primary source of brGDGTs, likely soil.

5.3. Provenance of the GDGT signal

Reconstructions of past continental climate have been based on indices and proxies derived from brGDGT distributions retrieved from paleosol-loess sequences (Peterse et al., 2011, 2014; Zech et al., 2012) and deltaic and river-proximal continental margin sediments (Weijers et al., 2007a; Sanchi et al., 2015). However, constraining the provenance of proxy signals is a prerequisite for accurate reconstruction of environmental conditions in sediment deposits. While certain inorganic and mineralogical properties of fluvial sediments integrate inputs from a river catchment and reflect basin-wide signals (Martin and Meybeck, 1979), organic matter turnover is much faster and therefore the particulate organic matter load that is discharged to the ocean may not carry an average basin-wide signal. Sanchi et al. (2015) reconstructed soil pH variations over the past 40 ka from a sediment core in the northwestern Black Sea and found a shift from Dnieper-dominated sediments toward a dominant sediment supply from the Danube at ca. 15.5 ka BP. However, this apparent shift in source region of brGDGT signals can only be explained if the alkaline soils (higher pH) from the lower Danube basin serve as the major source to the Black Sea instead of the more acidic soils from the Carpathian Mountains. Our study of modern sediment deposits along the Danube River shows proximal signals of the brGDGT-derived proxies, following local temperature and soil pH, and only a weak influence from upstream sources. Similar conclusions are reported for another large river system, the Yangtze River (Li et al., 2015). The finding of a local, lower basin, signal being exported from the Danube supports the interpretation of Sanchi et al. (2015), but underlines the importance of understanding signal provenance in interpretations of brGDGT-based paleoclimate investigations of fluvially dominated paleoclimate archives. In this context, further within-river investigations are clearly required to understand the evolution and origin of brGDGT and other molecular proxy signals as a function of climate and drainage basin properties.

6. Conclusions

The comparison of methods for brGDGT analysis of fluvial sediments undertaken here shows that improved chromatographic separation of pH- and temperature-dependent isomers leads to more accurate reconstruction of local environmental conditions. Applying this new method, we find that longitudinal trends in brGDGT-based mean annual air temperature and soil pH from fluvial sediments within the Danube River basin follow the actual local conditions from headwater tributaries to the Black Sea. Minor contributions from in situ derived brGDGTs do not significantly alter the signal derived from local soil inputs. We therefore conclude that the brGDGT signal ultimately exported to the Black Sea emanates from soils within the drainage basin, albeit dominated by inputs from the lower Danube basin.

Acknowledgements

This project was funded by the Swiss National Science Foundation (''CAPS-LOCK''; #200021_140850). We wish to thank everyone who took part in the sampling campaign (Björn Buggle, Marilu Tavagna, Alissa Zuijdgeest, James Saenz, Stefan Eugen Filip, Silvia Lavinia Filip and Mihai). Further acknowledgement goes to Daniel Montluçon, Negar Haghipour (ETH Zürich) and Dominika Kasjaniuk (UU) for laboratory support. This product includes data licensed from International Commission for the Protection of the Danube River (ICPDR) and data from FAO/IIASA/ISRIC/ISS-CAS/JRC. FP acknowledges ETH Fellowship FEL-36 11-1 and NWO Veni grant 863.13.016 for funding. NWO grant 834.11.006 enabled the purchase of the UHPLC-MS system for GDGT analysis at Utrecht University. This manuscript benefited from reviews by Cindy De Jonge, David Naafs and two anonymous reviewers.

Appendix A. Supplementary material

Supplementary data associated with this article can be found, in the online version, at http://dx.doi.org/10.1016/j.orggeochem.2016.11.002.

Associate Editor—**Sylvie Derenne**

References

Bendle, J.A., Weijers, J.W.H., Maslin, M.A., Sinninghe Damsté, J.S., Schouten, S., Hopmans, E.C., Boot, C.S., Pancost, R.D., 2010. Major changes in glacial and Holocene terrestrial temperatures and sources of organic carbon recorded in the Amazon fan by tetraether lipids. Geochemistry, Geophysics, Geosystems 11. http://dx.doi.org/10.1029/2010GC003308.

Buckles, L.K., Weijers, J.W.H., Tran, X.M., Waldron, S., Sinninghe Damsté, J.S., 2014. Provenance of tetraether membrane lipids in a large temperate lake (Loch Lomond, UK): implications for glycerol dialkyl glycerol tetraether (GDGT)-based palaeothermometry. Biogeosciences 11, 5539–5563.

Dang, X.Y., Yang, H., Naafs, B.D.A., Pancost, R.D., Xie, S.C., 2016. Evidence of moisture control on the methylation of branched glycerol dialkyl glycerol tetraethers in semi-arid and arid soils. Geochimica et Cosmochimica Acta 189, 24–36.

De Jonge, C., Hopmans, E.C., Stadnitskaia, A., Rijpstra, W.I.C., Hofland, R., Tegelaar, E., Sinninghe Damsté, J.S., 2013. Identification of novel penta- and hexamethylated branched glycerol dialkyl glycerol tetraethers in peat using HPLC–MS^2, GC–MS and GC–SMB–MS. Organic Geochemistry 54, 78–82.

De Jonge, C., Hopmans, E.C., Zell, C.I., Kim, J.H., Schouten, S., Sinninghe Damsté, J.S., 2014a. Occurrence and abundance of 6-methyl branched glycerol dialkyl glycerol tetraethers in soils: implications for palaeoclimate reconstruction. Geochimica et Cosmochimica Acta 141, 97–112.

De Jonge, C., Stadnitskaia, A., Hopmans, E.C., Cherkashov, G., Fedotov, A., Sinninghe Damsté, J.S., 2014b. In situ produced branched glycerol dialkyl glycerol tetraethers in suspended particulate matter from the Yenisei River, Eastern Siberia. Geochimica et Cosmochimica Acta 125, 476–491.

De Jonge, C., Stadnitskaia, A., Hopmans, E.C., Cherkashov, G., Fedotov, A., Streletskaya, I.D., Vasiliev, A.A., Sinninghe Damsté, J.S., 2015. Drastic changes in the distribution of branched tetraether lipids in suspended matter and sediments from the Yenisei River and Kara Sea (Siberia): implications for the use of brGDGT-based proxies in coastal marine sediments. Geochimica et Cosmochimica Acta 165, 200–225.

Ding, S., Xu, Y., Wang, Y., He, Y., Hou, J., Chen, L., He, J.S., 2015. Distribution of branched glycerol dialkyl glycerol tetraethers in surface soils of the Qinghai-Tibetan Plateau: implications of brGDGTs-based proxies in cold and dry regions. Biogeosciences 12, 3141–3151.

Giosan, L., Coolen, M.J.L., Kaplan, J.O., Constantinescu, S., Filip, F., Filipova-Marinova, M., Kettner, A.J., Thom, N., 2012. Early anthropogenic transformation of the Danube-Black Sea system. Scientific Reports 2. http://dx.doi.org/10.1038/srep00582.

Grams, C.M., Binder, H., Pfahl, S., Piaget, N., Wernli, H., 2014. Atmospheric processes triggering the central European floods in June 2013. Natural Hazards and Earth Systems Sciences 14, 1691–1702.

Hopmans, E.C., Schouten, S., Sinninghe Damsté, J.S., 2016. The effect of improved chromatography on GDGT-based palaeoproxies. Organic Geochemistry 93, 1–6.

Hopmans, E.C., Weijers, J.W.H., Schefuss, E., Herfort, L., Sinninghe Damsté, J.S., Schouten, S., 2004. A novel proxy for terrestrial organic matter in sediments based on branched and isoprenoid tetraether lipids. Earth and Planetary Science Letters 224, 107–116.

Huguet, A., Gocke, M., Derenne, S., Fosse, C., Wiesenberg, G.L.B., 2013. Root-associated branched tetraether source microorganisms may reduce estimated paleotemperatures in subsoil. Chemical Geology 356, 1–10.

Huguet, C., Hopmans, E.C., Febo-Ayala, W., Thompson, D.H., Sinninghe Damsté, J.S., Schouten, S., 2006. An improved method to determine the absolute abundance of glycerol dibiphytanyl glycerol tetraether lipids. Organic Geochemistry 37, 1036–1041.

HWSD, 2012. FAO/IIASA/ISRIC/ISS-CAS/JRC, Harmonized World Soil Database (version 1.2), FAO, Rome, Italy and IIASA, Laxenburg, Austria. <http://webarchive.iiasa.ac.at/Research/LUC/External-World-soil-database/HTML/> (date accessed: 04.08.2016).

ICPDR, 2005. The Danube River Basin District. Part A – basin-wide overview. In: Schmedtje, U. (Ed.), International Commission for the Protection of the Danube River, ICPDR.

ICPDR, 2014. Floods in June 2013 in the Danube River Basin – Brief Overview of Key Events and Lessons Learned.

JDS3, 2013. Danubis, the ICPDR Information System – Danube River Basin Water Quality Database. <http://www.icpdr.org/wq-db> (date accessed: 09.03.2016).

Kideys, A.E., 2002. Fall and rise of the Black Sea ecosystem. Science 297, 1482–1484.

Li, J.J., Pancost, R.D., Naafs, B.D.A., Yang, H., Zhao, C., Xie, S.C., 2016. Distribution of glycerol dialkyl glycerol tetraether (GDGT) lipids in a hypersaline lake system. Organic Geochemistry 99, 113–124.

Li, Z.Q., Peterse, F., Wu, Y., Bao, H.Y., Eglinton, T.I., Zhang, J., 2015. Sources of organic matter in Changjiang (Yangtze River) bed sediments: preliminary insights from organic geochemical proxies. Organic Geochemistry 85, 11–21.

Martin, J.M., Meybeck, M., 1979. Elemental mass-balance of material carried by major world rivers. Marine Chemistry 7, 173–206.

McCarney-Castle, K., Voulgaris, G., Kettner, A.J., Giosan, L., 2012. Simulating fluvial fluxes in the Danube watershed: the 'Little Ice Age' versus modern day. Holocene 22, 91–105.

Oppermann, B.I., Michaelis, W., Blumenberg, M., Frerichs, J., Schulz, H.M., Schippers, A., Beaubien, S.E., Kruger, M., 2010. Soil microbial community changes as a result of long-term exposure to a natural CO_2 vent. Geochimica et Cosmochimica Acta 74, 2697–2716.

Peterse, F., Martinez-Garcia, A., Zhou, B., Beets, C.J., Prins, M.A., Zheng, H.B., Eglinton, T.I., 2014. Molecular records of continental air temperature and monsoon precipitation variability in East Asia spanning the past 130,000 years. Quaternary Science Reviews 83, 76–82.

Peterse, F., Prins, M.A., Beets, C.J., Troelstra, S.R., Zheng, H.B., Gu, Z.Y., Schouten, S., Sinninghe Damsté, J.S., 2011. Decoupled warming and monsoon precipitation in East Asia over the last deglaciation. Earth and Planetary Science Letters 301, 256–264.

Peterse, F., van der Meer, J., Schouten, S., Weijers, J.W.H., Fierer, N., Jackson, R.B., Kim, J.H., Sinninghe Damsté, J.S., 2012. Revised calibration of the MBT-CBT paleotemperature proxy based on branched tetraether membrane lipids in surface soils. Geochimica et Cosmochimica Acta 96, 215–229.

Prado, A., Dacosta, M.S., Madeira, V.M.C., 1988. Effect of growth temperature on the lipid-composition of 2 strains of *Thermus* sp. Journal of General Microbiology 134, 1653–1660.

Sanchi, L., Menot, G., Bard, E., 2014. Insights into continental temperatures in the northwestern Black Sea area during the Last Glacial period using branched tetraether lipids. Quaternary Science Reviews 84, 98–108.

Sanchi, L., Menot, G., Bard, E., 2015. Environmental controls on paleo-pH at mid-latitudes: a case study from Central and Eastern Europe. Palaeogeography, Palaeoclimatology, Palaeoecology 417, 458–466.

Schouten, S., Hopmans, E.C., Sinninghe Damsté, J.S., 2013. The organic geochemistry of glycerol dialkyl glycerol tetraether lipids: a review. Organic Geochemistry 54, 19–61.

Schouten, S., Hopmans, E.C., van der Meer, J., Mets, A., Bard, E., Bianchi, T.S., Diefendorf, A., Escala, M., Freeman, K.H., Furukawa, Y., Huguet, C., Ingalls, A., Menot-Combes, G., Nederbragt, A.J., Oba, M., Pearson, A., Pearson, E.J., Rosell-Mele, A., Schaeffer, P., Shah, S.R., Shanahan, T.M., Smith, R.W., Smittenberg, R., Talbot, H.M., Uchida, M., Van Mooy, B.A.S., Yamamoto, M., Zhang, Z.H., Sinninghe Damsté, J.S., 2009. An interlaboratory study of TEX_{86} and BIT analysis using high-performance liquid chromatography–mass spectrometry. Geochemistry, Geophysics, Geosystems 10. http://dx.doi.org/10.1029/2008GC002221.

Schouten, S., Huguet, C., Hopmans, E.C., Kienhuis, M.V.M., Sinninghe Damsté, J.S., 2007. Analytical methodology for TEX_{86} paleothermometry by high-performance liquid chromatography/atmospheric pressure chemical ionization-mass spectrometry. Analytical Chemistry 79, 2940–2944.

Sinninghe Damsté, J.S., Ossebaar, J., Schouten, S., Verschuren, D., 2012. Distribution of tetraether lipids in the 25-ka sedimentary record of Lake Challa: extracting reliable TEX_{86} and MBT/CBT palaeotemperatures from an equatorial African lake. Quaternary Science Reviews 50, 43–54.

Sinninghe Damsté, J.S., Rijpstra, W.I.C., Hopmans, E.C., Foesel, B.U., Wust, P.K., Overmann, J., Tank, M., Bryant, D.A., Dunfield, P.F., Houghton, K., Stott, M.B., 2014. Ether- and ester-bound iso-diabolic acid and other lipids in members of acidobacteria subdivision 4. Applied and Environment Microbiology 80, 5207–5218.

Sinninghe Damsté, J.S., Rijpstra, W.I.C., Hopmans, E.C., Weijers, J.W.H., Foesel, B.U., Overmann, J., Dedysh, S.N., 2011. 13,16-Dimethyl octacosanedioic acid (iso-diabolic acid), a common membrane-spanning lipid of acidobacteria subdivisions 1 and 3. Applied and Environment Microbiology 77, 4147–4154.

Suutari, M., Laakso, S., 1992. Temperature adaptation in *Lactobacillus fermentum*: interconversions of oleic, vaccenic and dihydrosterulic acids. Journal of General Microbiology 138, 445–450.

Tierney, J.E., Russell, J.M., 2009. Distributions of branched GDGTs in a tropical lake system: implications for lacustrine application of the MBT/CBT paleoproxy. Organic Geochemistry 40, 1032–1036.

Tierney, J.E., Schouten, S., Pitcher, A., Hopmans, E.C., Sinninghe Damsté, J.S., 2012. Core and intact polar glycerol dialkyl glycerol tetraethers (GDGTs) in Sand Pond, Warwick, Rhode Island (USA): insights into the origin of lacustrine GDGTs. Geochimica et Cosmochimica Acta 77, 561–581.

Tockner, K., Uehlinger, U., Robinson, C.T., 2009. Rivers of Europe. Elsevier Science.

Weber, Y., De Jonge, C., Rijpstra, W.I.C., Hopmans, E.C., Stadnitskaia, A., Schubert, C.J., Lehmann, M.F., Sinninghe Damsté, J.S., Niemann, H., 2015. Identification and carbon isotope composition of a novel branched GDGT isomer in lake sediments: evidence for lacustrine branched GDGT production. Geochimica et Cosmochimica Acta 154, 118–129.

Weijers, J.W.H., Schouten, S., van der Linden, M., van Geel, B., Sinninghe Damsté, J.S., 2004. Water table related variations in the abundance of intact archaeal membrane lipids in a Swedish peat bog. FEMS Microbiology Letters 239, 51–56.

Weijers, J.W.H., Schefuss, E., Schouten, S., Sinninghe Damsté, J.S., 2007a. Coupled thermal and hydrological evolution of tropical Africa over the last deglaciation. Science 315, 1701–1704.

Weijers, J.W.H., Schouten, S., van den Donker, J.C., Hopmans, E.C., Sinninghe Damsté, J.S., 2007b. Environmental controls on bacterial tetraether membrane lipid distribution in soils. Geochimica et Cosmochimica Acta 71, 703–713.

Weijers, J.W.H., Wiesenberg, G.L.B., Bol, R., Hopmans, E.C., Pancost, R.D., 2010. Carbon isotopic composition of branched tetraether membrane lipids in soils suggest a rapid turnover and a heterotrophic life style of their source organism (s). Biogeosciences 7, 2959–2973.

Xiao, W.J., Xu, Y.P., Ding, S., Wang, Y.H., Zhang, X.Y., Yang, H., Wang, G.A., Hou, J.Z., 2015. Global calibration of a novel, branched GDGT-based soil pH proxy. Organic Geochemistry 89–90, 56–60.

Yang, G., Zhang, C.L., Xie, S., Chen, Z., Gao, M., Ge, Z., Yang, Z., 2013. Microbial glycerol dialkyl glycerol tetraethers from river water and soil near the Three Gorges Dam on the Yangtze River. Organic Geochemistry 56, 40–50.

Zech, R., Gao, L., Tarozo, R., Huang, Y., 2012. Branched glycerol dialkyl glycerol tetraethers in Pleistocene loess-paleosol sequences: three case studies. Organic Geochemistry 53, 38–44.

Zell, C., Kim, J.H., Hollander, D., Lorenzoni, L., Baker, P., Silva, C.G., Nittrouer, C., Sinninghe Damsté, J.S., 2014. Sources and distributions of branched and isoprenoid tetraether lipids on the Amazon shelf and fan: implications for the use of GDGT-based proxies in marine sediments. Geochimica et Cosmochimica Acta 139, 293–312.

Zell, C., Kim, J.H., Moreira-Turcq, P., Abril, G., Hopmans, E.C., Bonnet, M.P., Sobrinho, R.L., Sinninghe Damsté, J.S., 2013. Disentangling the origins of branched tetraether lipids and crenarchaeol in the lower Amazon River: implications for GDGT-based proxies. Limnology and Oceanography 58, 343–353.